We are IntechOpen,
the world's leading publisher of
Open Access books
Built by scientists, for scientists

4,400
Open access books available

117,000
International authors and editors

130M
Downloads

154
Countries delivered to

Our authors are among the

TOP 1%
most cited scientists

12.2%
Contributors from top 500 universities

BOOK CITATION INDEX
CLARIVATE ANALYTICS
INDEXED

WEB OF SCIENCE™

Selection of our books indexed in the Book Citation Index
in Web of Science™ Core Collection (BKCI)

Interested in publishing with us?
Contact book.department@intechopen.com

Numbers displayed above are based on latest data collected.
For more information visit www.intechopen.com

Optical Properties of Complex Oxide Thin Films Obtained by Pulsed Laser Deposition

Valentin Ion, Andreea Andrei, Maria Dinescu and
Nicu Doinel Scarisoreanu

Additional information is available at the end of the chapter

Abstract

The market for thin films of complex oxides obtained by different deposition techniques is increasing exponentially in last decades due to large variety of possible application such as high-efficient solar cell, optoelectronic devices, etc. pulsed laser deposition (PLD) is a versatile growth technique and recently became more attractive for industrial applications due to the possibility to obtain crystalline thin films on a large area. Laser processing techniques were successfully used to obtain thin films with good optical properties starting from simple oxides, such as Sm_2O_3, ZrO_2, etc., to more complex lead-free materials: $Sr_xBa_{1-x}Nb_2O_6$ (SBN) and $Na_{1/2}Bi_{1/2}TiO_3-x\%BaTiO_3$, or superconductive oxide $YBa_2Cu_3O_{7-\delta}$. When oxide thin films are designated for electronic and optoelectronic devices or for solar cells, the optical properties and the thickness must be well known. For this purpose, the spectroscopic ellipsometry technique was developed. Ellipsometry is a powerful technique to determine the optical properties of thin films especially when the thicknesses of thin films are in a nanometer range.

Keywords: spectroscopic ellipsometry, pulsed laser deposition, thin films, complex oxides, magnetic alloy, high temperature superconductor

1. Introduction

A thin film is a layer of material, which can be created by various processes, one of the most common being the condensation of particles (atoms, molecules, ions, aggregates) on a substrate. The thickness of the layer can vary between few angstroms (monolayer) and several micrometers. The market for thin films obtained by different deposition techniques had an exponential increase in the last decades due to the large variety of possible applications, such as hard coatings, semiconductor devices, optical coatings, energy generation and storage, memory devices, sensors, actuators, etc.

Thin film deposition techniques are divided in two major categories: chemical vapor deposition (CVD) and physical vapor deposition (PVD) [1, 2]. Pulsed laser deposition (PLD), developed by Maiman, Smith, and Turner, in the 1960s, is a PVD technique based on laser-material interaction [3–5]. It is a versatile technique and recently became more attractive for industrial applications due to the possibility to obtain crystalline thin films on large areas. Laser processing techniques were successfully used to obtain thin films from all kind of materials, starting from alloys (NdFeB), simple oxides (Sm_2O_3, ZrO_2, etc.), to more complex materials: high temperature superconductors ($YBa_2Cu_3O_{7-\delta}$), ferroelectric $Sr_xBa_{1-x}Nb_2O_6$ with tungsten bronze structure or solid solution of $Na_{1/2}Bi_{1/2}TiO_3$–x%$BaTiO_3$, etc.

The basic setup for pulsed laser deposition is relatively simple, but the physical phenomena of laser-matter interaction and film growth are very complex [5]. Because thin films have a large surface area to bulk volume ratio, their physical and chemical properties can be different from the bulk materials [6]. The substrate properties and the deposition parameters during the grown process can drastically influence the properties of thin films. By carefully choosing these parameters, thin films with enhanced physical properties can be obtained.

The properties of thin films can be investigated by various analysis techniques. X-ray diffraction (XRD) and transmission electron microscopy (TEM) are used for structural investigation, scanning electron microscopy (SEM) and atomic force microscopy (AFM) for morphological analysis, secondary ion mass spectroscopy (SIMS) for compositional analysis, etc. Electrical and optical properties are also very important when thin films are designated to be used in electronic, opto-electronic, or optical applications. For optical investigation, ellipsometry is a very precise and fast method, especially when the thickness of the thin films ranges from subnanometers to hundreds of nanometers.

In Section 2, a short overview of the principles and analysis procedures of ellipsometry are presented. In Section 3, a review of the optical investigation of thin films obtained by PLD is presented. Finally, conclusions are given in Section 4.

2. Ellipsometry

The history of ellipsometry is difficult to trace precisely. It can be said that it starts with the "wave theory of light" of Robert Hooke followed by the contribution of many scientists: Christian Huygens, Augustin-Jean Fresnel, Michael Faraday, James Clerk Maxwell, etc. In 1902, Paul Drude published the "Polarization" chapter in the book "The Theory of Optics," which still serves as a modern introduction to the study of polarized light and ellipsometry [7]. Ellipsometry developed slowly for long time after the Drude ellipsometer, using a single wavelength in the 1960s. After 1970, due to the necessity of faster measurements for thin films used in computers or the semiconductor industry, the ellipsometry techniques developed rapidly [8, 9]. Nowadays, there are many types of ellipsometers, such as null, photometric, spectroscopic, etc.

Ellipsometry is a tool that gives information about the optical properties and microstructural parameters of materials, such as layer thicknesses, porosity, and crystalline state. Ellipsometry is a nondestructive, fast, sensitive, and accurate technique used to determine the optical constants of a large range of materials: metals, glasses, complex oxide structures, polymers,

organic materials, etc. It can be used for ex-situ or in-situ analysis, both for inorganic and organic materials. However, a major disadvantage of this technique is that it is an indirect analysis, and an accurate optical model is required for data analysis.

2.1. Principle and analysis procedure of ellipsometry

In the past decades, many books and scientific papers regarding the principle, data analysis procedure, and applications of ellipsometry were published [8, 10–13]. In this section, we present a brief overview of the ellipsometry principles and data acquisition and analysis procedure.

In ellipsometry, the change of the polarization state of linearly polarized light is measured upon reflection at the surface of a sample. The polarization states after reflection depend on properties of the investigated surface and, in case of multilayer thin film system, on the properties of each layer. Two experimental parameters, ψ and Δ, called ellipsometric angles, are usually measured (**Figure 1**).

Here, ψ is the relative amplitude and Δ is the phase difference for p- and s-polarized lights, and the quantities ψ and Δ are described by the fundamental equation of ellipsometry (Eq. (1)),

$$\rho = \frac{\tilde{R}_p}{\tilde{R}_s} = \tan(\Psi)e^{i\Delta} = \left(\frac{E_{rp}/E_{ip}}{E_{rs}/E_{is}}\right), \tag{1}$$

where R_p and R_s are the Fresnel reflection coefficients; E_{rp}, E_{is}, E_{rp}, and E_{rs} represent the p- and s-components of the incident and reflected light waves. The p- and s-polarization terms represent the parallel (p) and the perpendicular (s) components of electric field, related to the incidence plane.

In case of thin films, the incident light is reflected on the thin film surface and penetrates into the film and into the substrate. An obtained ellipsometric data include information about the
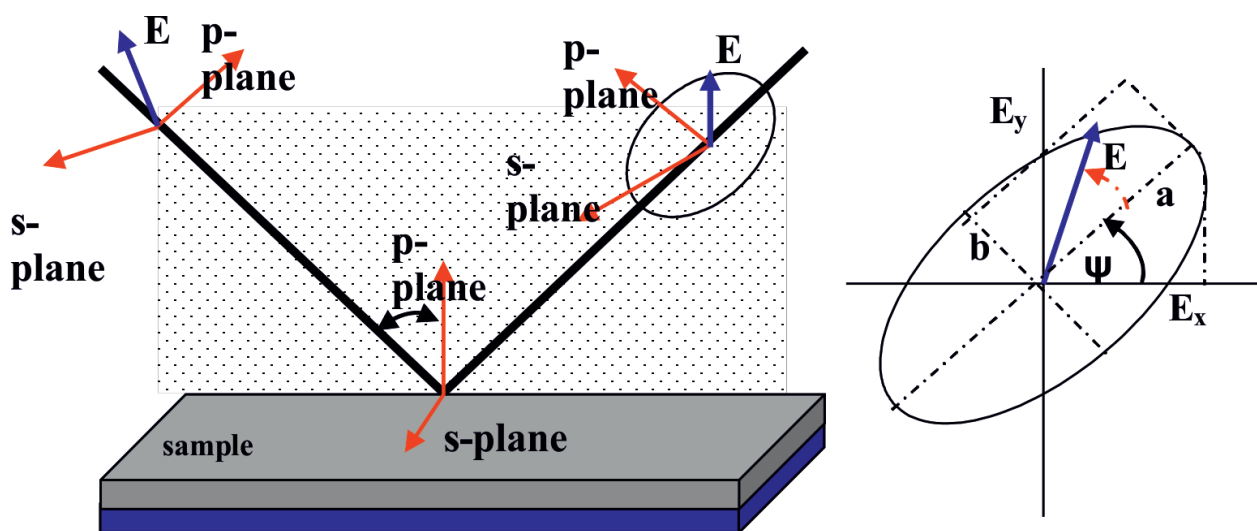

Figure 1. Scheme showing the basic principle of ellipsometry: linearly polarized light with p- and s-components at oblique incidence is reflected and it becomes elliptically polarized. Relative attenuation of s- and p-polarized lights eterminates the tilt of the ellipse and the relative phase shift is related to ellipticity [12].

investigated materials. For a thin film deposited on a substrate, $\varrho = F(n_0, n_1, n_2, \theta, d)$ where n_0, n_1, and n_2 are the complex refractive indices of the ambient, the thin film, and the substrate, θ is the angle of incidence of the light beam, and d is the thickness of the thin layer (**Figure 2**).

The complex refractive index is composed by a real part "n" and by an imaginary part "k" The imaginary part is called the extinction coefficient and is directly related to absorption of the light in the material. The absorption coefficient is given by $\alpha = 4\pi k/\lambda$, where λ is the free-space wavelength of light. The complex dielectric function $\varepsilon = \varepsilon_1 - i\varepsilon_2$ and the complex index of refraction N are related to each other through the relation derived from Maxwell's equations [11, 12]: $\varepsilon = N^2$. The real and imaginary parts are: $\varepsilon_1 = n^2 - k^2$ and $\varepsilon_2 = 2nk$. Since ellipsometry measures changes in the polarization state, this makes it a highly accurate and reproducible technique. Ψ and Δ can be determined experimentally with high precision, but the extraction of information (optical constants and thickness) requires, for calculation, an accurate optical model.

In case of thin film system, the purpose of ellipsometry measurement is to determine the optical properties of the materials from the measured Ψ and Δ parameters. The refractive index, extinction coefficient, and thickness of each layer can be determined. **Figure 3** shows the process of ellipsometry analysis procedure.

The standard procedure of analysis includes the following steps.
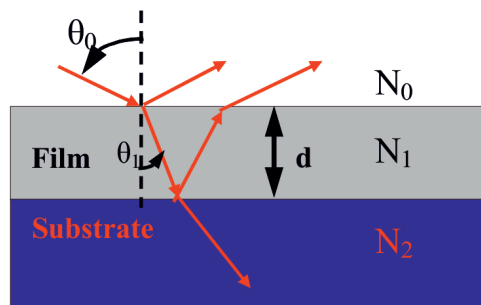
Figure 2. The optical model for thin film system.
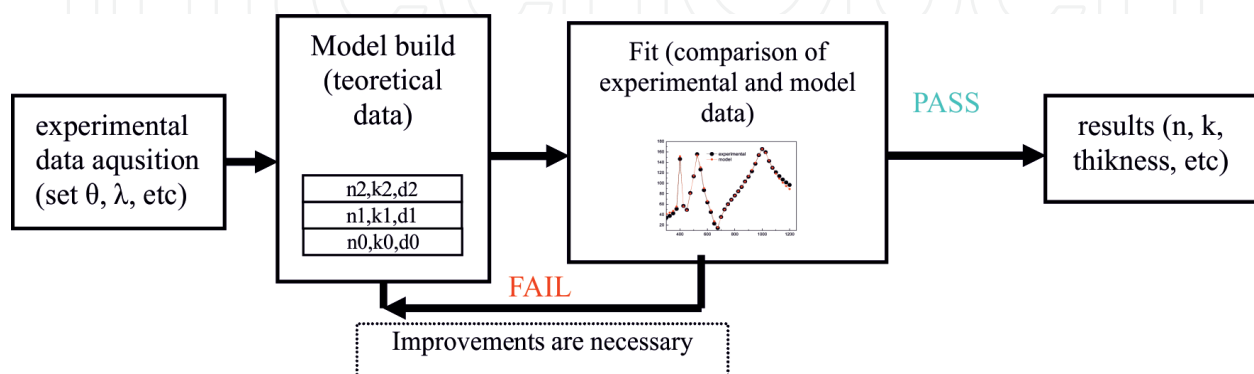
Figure 3. Process of ellipsometry data fitting and model analysis.

2.1.1. The experimental measurement

In this step, the routine of experimental data point acquisition is established. The set-up parameters include the wavelength, the number of experimental data points, and the angle of incidence. For spectroscopic ellipsometry, measurements are done in a large wavelength spectrum, ranging from deep ultraviolet (UV) to near infrared (IR) (i.e., 250–1700 nm).

2.1.2. The optical model

A suitable optical model is required for ellipsometric analysis. In case of thin films, the optical model is composed by a stack of several kinds of material layers with different thicknesses. The properties of material layers are described by a specific complex dielectric function. Usually, at this point, the dielectric function of the substrate is known. If not, a separate analysis is required for bulk substrate. In the optical model, some of the parameters are unknown, such as the thickness or the values of optical constants. For optical characterization of thin films, it is necessary to select a suitable dispersion model. Examples of dispersion models are Cauchy dispersion with Urbach tail, Sellimeier model, effective medium approximation (EMA), Drude model or Lorentz model, etc. In order to find what dispersion model should be selected for a thin film depends on the types of materials.

2.1.3. Comparison of model and experimental data

Using the optical model, the values of theoretical Ψ and Δ are generated and compared with the experimental data. If the graphs of both data match, the optical model can be considered correct. The following function is usually employed for the comparison (Eq. (2)):

$$\text{MSE} = \frac{1}{2N - M} \sum_{i=1}^{N} \left[\left(\frac{\Psi_i^{\text{mod}} - \Psi_i^{\text{exp}}}{\sigma_{\psi, i}^{\text{exp}}} \right)^2 + \left(\frac{\Delta_i^{\text{mod}} - \Delta_i^{\text{exp}}}{\sigma_{\Delta, i}^{\text{exp}}} \right)^2 \right], \tag{2}$$

where N is the number of (Ψ, Δ) pairs, M is the number of variable parameters in the model, and σ is the standard deviations on the experimental data points.

The MSE, as shown in the equation, represents a sum of the squares of differences between the measured and calculated data, with each difference weighted by the standard deviation of that measured data point. The unknown parameters in the optical model are varied in order to produce a good fit. The best fit will lead to minimum of the MSE value. In case of "bad" match of theoretical and experimental data, or high value of MSE, the optical model will be adjusted until the minimum value of MSE is reached. After obtaining the best fit and the minimum of MSE value, the values of the optical constants can be generated. The dispersion of optical constants needs to be physically reasonable regarding the analyzed thin film materials.

As mentioned before, for optical characterization of thin films, it is necessary to select a suitable dispersion model, and this model depends on the analyzed material. The values of the refractive index, the extinction coefficients, and the thickness of the thin film are considered as unknown parameters. Also, the optical model will usually include a distinct top layer, which accounts for the roughness of the thin film.

In many cases, the analyzed materials are UV-absorbing, such as semiconductors, metal oxides, or ferroelectric or multiferroic materials. For these materials, a common routine for ellipsometric analysis can be given. When the film is transparent over a portion of measured spectral range, it is possible to determine the thickness of the film with high accuracy using a Cauchy or Sellmeier dispersion model. In the next step, the thickness and Cauchy parameters values will be kept fixed, and the experimental data will be fitted point by point across the entire measured spectral range. In this way, a set of optical constants is obtained. The final values of optical constants (or dielectric function) will be obtained by replacing the Cauchy model with a sum of oscillators. Fitting again the experimental data, the parameters of the oscillators will be determined. For example, in case of Lorentz or Gauss oscillators, the parameters are as follows: the oscillation amplitude, the broadening, and the position of oscillation. After the oscillator parameters are known, the thickness will be fitted again for final adjustment. Ellipsometry is quite sensitive to the surface structure and is necessary to incorporate a rough top layer in the optical model in the data analysis.

Once the unknown parameters of thin film are determined, the value of thickness and dielectric function of the rough top layer will be calculated. It is rather difficult to estimate the complex refractive index of the roughness layer. The rough top layer is composed by a mix of thin film materials and air or voids.

If we apply the effective medium approximation (EMA), the complex refractive indices of surface roughness layer can be calculated [14]. In case of thin films, a percent of 50:50 (voids: material) in Bruggeman effective medium approximation (BEMA) is a good approximation for the composition of the rough top layer. The Bruggeman effective medium approximation (BEMA) is expressed by the following equation (Eq. (3)):

$$f_A \frac{\tilde{\varepsilon}_A - \tilde{\varepsilon}}{\tilde{\varepsilon}_A + 2\tilde{\varepsilon}} + f_B \frac{\tilde{\varepsilon}_B - \tilde{\varepsilon}}{\tilde{\varepsilon}_B + 2\tilde{\varepsilon}} = 0, \tag{3}$$

where f_A and f_B are the volume ratios of media A and B, and ε_A and ε_B are the complex dielectric functions of media A and B.

In the next section, we will present some examples of ellipsometric analysis on thin films obtained by pulsed laser techniques, starting from simple oxide materials, magnetic, to more complex ferroelectric thin films, evidencing in this way the capability of this technique.

3. Results and discussion

3.1. Experimental set-up

3.1.1. Pulsed laser deposition (PLD)

The experimental set-up for PLD experiment is based on two main equipments: a laser system and a vacuum chamber. The used laser systems were a Nd:YAG laser and a ArF excimer laser. The targets and collector substrate are mounted in the chamber in a vertical position, at variable distance. The angle of incidence of the laser beam was set at 45°. The substrates were fixed on a heating system. During deposition, the targets were rotated and the laser beam was

translated on surface of the targets. The film deposition was performed in a dynamic ambient background gas (O_2, N_2, etc.) and the flow rates of gases were precisely controlled through a MKS mass flow controller. All substrates used in the experiments were commercial substrates and before the experiments were cleaned in an ultrasonic bath using acetone or methanol as cleaning agents, then dried under pressurized nitrogen gas.

3.1.2. Spectroscopic ellipsometry

Optical measurements were performed with a Woollam variable angle spectroscopic ellipsometer (VASE) system, equipped with a high pressure Xe discharge lamp incorporated in an HS-190 monochromator. The ellipsometry measurements and analysis were done using the VASE32 software. Usually, the experimental data of Ψ and Δ were acquired in the 250–1700 nm range of wavelengths, with a step of 2 nm. The angle of incidence of the light beam was set in function of the analyzed materials, from 60 to 75° with a step of 5°.

3.1.3. Samarium oxide

Samarium oxide (Sm_2O_3) is a lanthanide oxide with a monoclinic structure. Sm_2O_3 is used as a neutron absorber in control rods for nuclear power reactors and in optical and infrared absorbing glass to absorb infrared radiation or as a gate dielectric in metal-oxide-semiconductor (MOS) devices [15, 16].

The target used in PLD experiments was prepared by pressing the Sm_2O_3 powder of 99.9% purity. For ellipsometry measurements, the substrate used was silicon. A laser beam from a pulsed Nd:YAG laser system (266 nm wavelength) was focused on the Sm_2O_3 target, with a laser spot of 0.8 mm^2 with 10 Hz repetition rate. The substrates were kept at room temperature during the depositions. The deposition was performed under the oxygen pressure range between 0.02 and 0.6 mbar.

Spectroscopic ellipsometry measurements were performed in the UV-visible and near-IR region of the spectrum (250–1350 nm), a step of 10 nm, at 60 and 65° angles of incidence. The optical model consists of five layers: the silicon substrate, the Si-SiO_2 interface, the native SiO_2 layer, the Sm_2O_3 layer, and a rough top layer. The rough top layer is set to be half air and half Sm_2O_3. The refractive indices for the substrate and the native oxide are from Herzinger et al. [17]. For optical constants of Sm_2O_3, we used the Cauchy dispersion model for transparent zone of wavelength, with Urbach tail for low absorbing region (below 400 nm). The Cauchy-Urbach model is given by the following equations (Eqs. (4) and (5)):

$$n(\lambda) = A_n + \frac{B_n}{\lambda^2} + \frac{C_n}{\lambda^4} \tag{4}$$

and

$$k = A_k \cdot e^{B(E-E_b)}, \tag{5}$$

where A_n, B_n, C_n, A_k, and B are constants and E is energy in eV (E = 1240/λ; E_b = 1240/λ_b).

Fitting the experimental data with Cauchy-Urbach dispersion model and assuming that the top layer consists of 50% air (voids) and 50% Sm_2O_3, we have obtained the parameters listed in **Table 1**:

Figure 4 presents the SE spectra of a 59.8 ± 0.3 nm thick Sm_2O_3 on silicon substrate with a roughness of 6.5 ± 0.3 nm, the optical constants n = 1.94 and $k = 6 \times 10^{-3}$, at $\lambda = 550$ nm, and the MSE = 4.55.

The surface topography was analyzed by AFM. The roughness of the thin film was found to be in nanometer range, excluding the droplets present on the film surface [18].

The obtained Sm_2O_3 thin films are highly transparent in the 400–1350 nm wavelength range. Below 400 nm, the film becomes optically absorbing, with a maximum extinction coefficient $k \sim 3 \times 10^{-2}$ (at 250 nm). The Sm_2O_3 is a high refractive index material, with a value of n = 2.09 at a wavelength of 589.3 nm and has a monoclinic crystalline phase. This value is with 0.1 larger than our value. The amorphous materials have a smaller refractive index than the crystalline material [11, 12], and our smaller value indicates an amorphous phase of Sm_2O_3 in the thin film, which is consistent with the XRD measurements [18].

As a short conclusion of this case: using a simple model such as Cauchy dispersion with Urbach tail, it is possible to obtain valuable information regarding the dispersion of optical constants, thickness, and the crystalline phase of the film. However, the Cauchy dispersion model is limited at the transparent range of wavelength, and the Urbach tail is limited at low absorption zone. To sum up: a correct value of optical band gap E_g cannot be given using this model.

3.1.4. Zirconia

Zirconia (ZrO_2) (zirconium dioxide) is a dielectric material with a dielectric constant of about 20 (in the low frequency domain). Because of its low leakage current level and high thermal

Sample	Thickness (nm)	Roughness (nm)	An	Bn	Ak	Bk	MSE
Sm_2O_3/Si	59.8 ± 0.22	6.5 ± 0.36	1.932 ± 0.002	0.016 ± 0.003	0.002 ± 0.001	1.343 ± 0.28	4.555

Table 1. The Cauchy-Urbach fit parameters for Sm_2O_3 thin film.
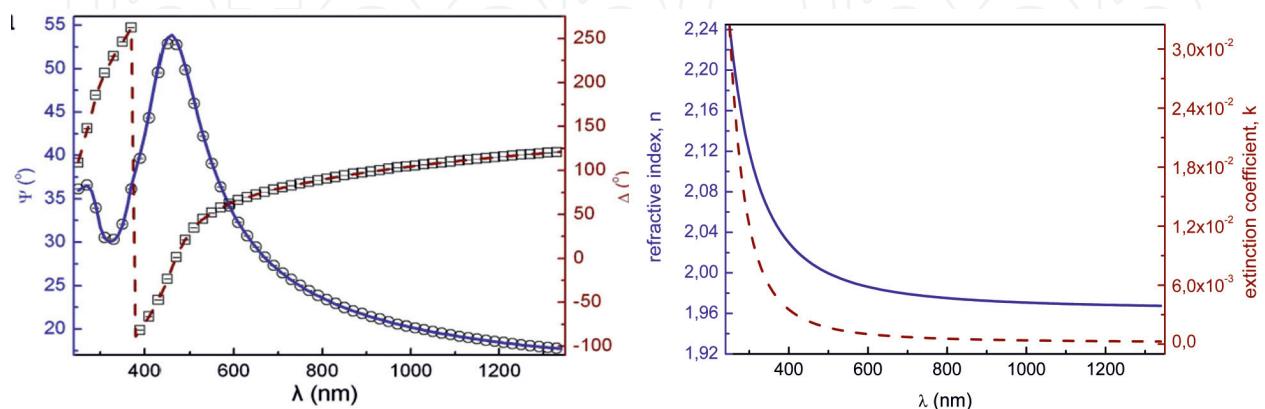
Figure 4. SE spectra on a Sm_2O_3 film: (left) the open symbols represent experimental data, whereas the solid line (Ψ) and dashed line (Δ) are obtained from a fitting procedure using a five-layer model and (right) the refractive index (solid line) and the extinction coefficient (dashed line) for the Sm_2O_3 thin films [18].

stability, ZrO_2 is another candidate used for gate dielectrics in metal-oxide-semiconductor (MOS) [19]. Pure ZrO_2 exists as three polymorphs at different temperatures: monoclinic, tetragonal, and cubic.

A ceramic target of ZrO_2 was ablated with an ArF laser beam (λ = 193 nm) at a repetition rate of 40 Hz. The laser fluences were varied in the range of 2.0–3.4 J/cm^{-2}. The silicon (Si) substrate was kept at a distance of 4 cm from the target. The substrate temperature was between room temperature and 600°C, in the presence of reactive oxygen at a pressure of 0.1 mbar. The reactive oxygen was introduced in the deposition chamber by an additional RF discharge at a power of 100 W.

Ellipsometric measurements were carried out in the spectral range of 250–1700 nm, in steps of 2 nm, and incident angles of 60, 65, and 70°. The optical model comprises the silicon substrate, a layer of native oxide of silicon (3 nm), the ZrO_2 thin film, and a roughness layer, approximated by 50% voids and 50% ZrO_2. For the substrate, we used the dielectric function from literature [17].

The calculation of the complex refractive index and the thickness of the thin film and the rough layer required a two-step fitting procedure. In the first step, a simple Cauchy dispersion model was used in the 500–1700 nm range of wavelength, where the ZrO_2 is transparent [20]. The values of thickness and Cauchy parameters are listed in **Table 2** [21].

In order to fit the entire measured spectra and to calculate the extinction coefficients, the values of thickness were kept fixed and the Cauchy dispersion model was replaced by a single Gaussian oscillator. The imaginary part of the dielectric function for Gauss oscillator is given by the following equations (Eqs. (6) and (7)):

$$\varepsilon_2 = A^{e^{-\left(\frac{E-E_n}{\sigma}\right)^2}} - A^{e^{-\left(\frac{E+E_n}{\sigma}\right)^2}} \tag{6}$$

and

$$\sigma = \frac{Br_n}{2\sqrt{\ln(2)}}, \tag{7}$$

where A is the amplitude of the curve's peak, En refers to the centering energy or energy at the curve's peak, Br is the broadening, and σ is the standard deviation of the curve [12]. The fitted result parameters are listed in **Table 3**.

Values of MSE obtained in the second step of fitting increase slightly from 5.94 for Cauchy fit for the thin film grown at 300°C to 9.67 for Gauss fit, but the difference is still small enough to

Sample/temperature (°C)	Thickness (nm)	Roughness (nm)	An	Bn	MSE
ZrO_2/Si (RT)	64.177 ± 0.0391	0.904 ± 0.06	1.9882 ± 0.000591	0.014203 ± 0.000156	1.908
ZrO_2/Si (300°C)	190.812 ± 0.0537	1.403 ± 0.0481	2.1417 ± 0.000256	0.018515 ± 0.000153	5.944
ZrO_2/Si (600°C)	154.380 ± 0.0384	2.047 ± 0.0429	2.1535 ± 0.000211	0.01856 ± 0.000192	4.815

Table 2. The Cauchy fit parameters for ZrO_2 thin film.

be taken into consideration. This difference can arise from small discrepancy between the model and the experimental curve in the UV region caused by small defects on the surface, such as droplets or pores.

In **Figure 5**, we can observe that the higher values of refractive index were obtained for a substrate temperature of T = 600°C and also for the highest value of extinction coefficients. At room temperature, the smaller value of "n" indicates an amorphous phase, and this is in agreement with XRD results [21]. The best optical constants in terms of high "n" and lower "k" were obtained at 300°C. From **Table 2**, the values of thickness of ZrO_2 thin films grown by PLD in the presence of RF discharge were found to be 64 nm for room temperature, 190 nm for 300°C, and 154 nm for 600°C. At this point, we can conclude that the best temperature for growing transparent ZrO_2 thin films is 300°C. The XRD results indicate the presence of two crystalline phases, tetragonal and monoclinic, for ZrO_2 thin film in case of 600°C substrate temperature [21]. Coexistence of these two phases indicates a polycrystalline grown mode and explains the higher value of extinction coefficient (for 600°C).

As a short conclusion of this case, using a simple Gauss model, it is possible to determine the behavior of complex refractive index in function of PLD deposition parameters.

3.1.5. NdFeB

NdFeB is a permanent magnet based on rare earth components and has been widely investigated for its applications in micromagnetic, magneto-electronic, or magnetic recording media.

Sample/temperature (°C)	Amp	En (eV)	Br (eV)	MSE
ZrO_2/Si (RT)	19.849 ± 5.15	8.9932 ± 0.137	1.9394 ± 0.525	4.533
ZrO_2/Si (300°C)	20.196 ± 1.41	8.841 ± 0.0585	2.2913 ± 0.171	9.675
ZrO_2/Si (600°C)	16.331 ± 0.338	9.1236 ± 0.0346	2.9503 ± 0.0698	9.783

Table 3. The Gauss fit parameters for ZrO_2 thin film.
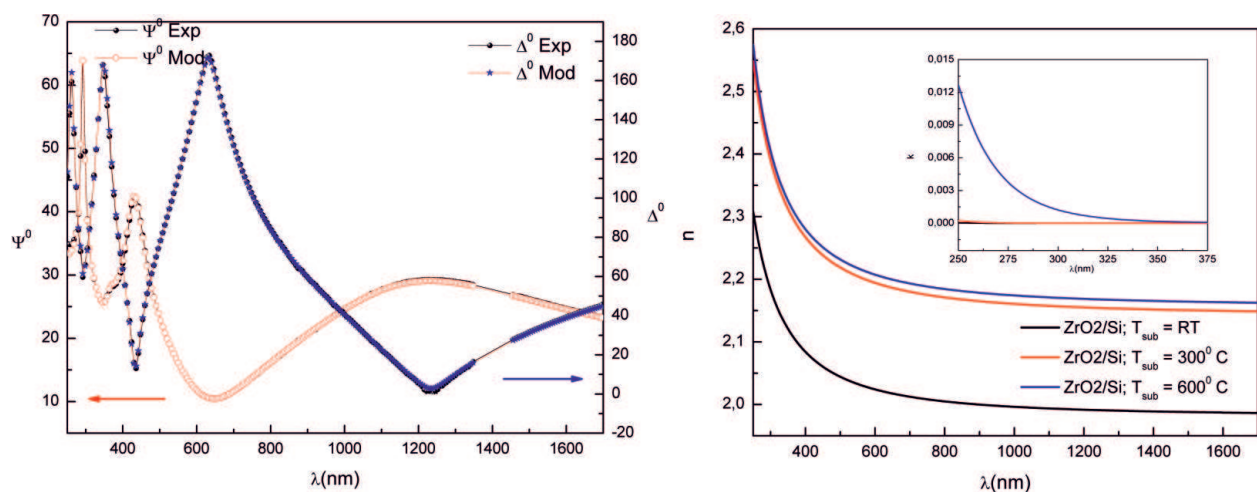
Figure 5. (Left) Experimental and Gauss-modeled curves for the parameters psi (Ψ) and delta (Δ) for an ZrO_2/Si(100) thin film deposited at 6000°C by RF-plasma-assisted PLD and (right) the dispersion of optical constants for ZrO_2 thin films grown at different substrate temperatures.

NdFeB thin films were deposited by various methods, e.g., magnetron sputtering, molecular beam epitaxy (MBE), and PLD [22–25].

In our experiments, the NdFeB thin films were obtained by PLD method [26] starting from an alloy target. A Nd:YAG laser (266 nm) was used to irradiate the targets with 20,000–40,000 pulses. The substrates were platinized silicon (Pt/Si). The samples were heated to 650°C, and the temperature was kept constant during the thin film growth.

Spectroscopic ellipsometry measurements were performed between 350 and 1700 nm spectral ranges, with a step of 2 nm at a fixed angle of incidence (75°). The initial optical model used to determine the complex refractive index consisted of a stack of five layers: the silicon substrate, the titanium layer (25 nm), the platinum layer (150 nm), the NdFeB layer, and the rough top layer. Because the platinum layer is thick enough, we considered this layer as a substrate and the optical model was reduced to three layers: Pt, NdFeB, and the rough layer. The values for the optical constants of NdFeB thin films were fitted using different procedures. The Cauchy-Urbach dispersion model used in case of Sm_2O_3 did not fit the NdFeB due to their limitation [11, 12]. The best fit was obtained with a Lorentz oscillator having the complex dielectric function (Eq. (8)) written as:

$$\varepsilon_{n-\mathrm{Lorentz}} = \frac{A_n Br_n E_n}{E_n^2 - E^2 - iBr_n E}, \tag{8}$$

where A_n is an oscillation amplitude (dimensionless), Br is broadening (expressed in eV), and E_n is the position of oscillation (eV). The total dielectric function is given by (Eq. (9)):

$$\varepsilon = \varepsilon_1 + i\varepsilon_2 = e_{1\mathrm{offset}} + \varepsilon_{n-\mathrm{Lorentz}}, \tag{9}$$

where $\varepsilon_{1\ \mathrm{offset}}$ is a purely real constant, equivalent to $\varepsilon_{\mathrm{inf.}}$ [12].

The Lorentz parameters and the thickness resulted from fitting experimental data with the proposed optical mode are presented in **Table 4**.

The thickness of a thin film deposited at 40,000 pulses, 266 nm laser wavelength, and 2 J/cm^2 laser fluency was found to be 93 nm with a roughness of 10 nm. For optical constants, a refractive index with a value of n = 2.43 was found for λ = 600 nm with a maximum of 2.46 at 360 nm. The extinction coefficient "k" is nonzero on the entire measured range of wavelength thin film that has high optical absorption [26].

The value of MSE is 31, and from **Figure 6**, it is easy to observe a mismatch between the experimental and the model data in UV-visible range. This mismatch indicates an improvement needed in the optical model. Even with this discrepancy, we have demonstrated that with a correct dispersion model (Lorentz in this case), it is possible to determine the complex optical constants for this magnetic thin film.

Thickness (nm)	Roughness (nm)	E_r (eV)	B_r (eV)	A_n	e1$_{\mathrm{offset}}$	MSE
93.609 ± 0.307	10.353 ± 0.221	5.7013 ± 0.208	4.2273 ± 0.217	3.1234 ± 0.169	3.3783 ± 0.13	31.3

Table 4. Spectroscopic ellipsometry fitted data for an NdFeB thin film.
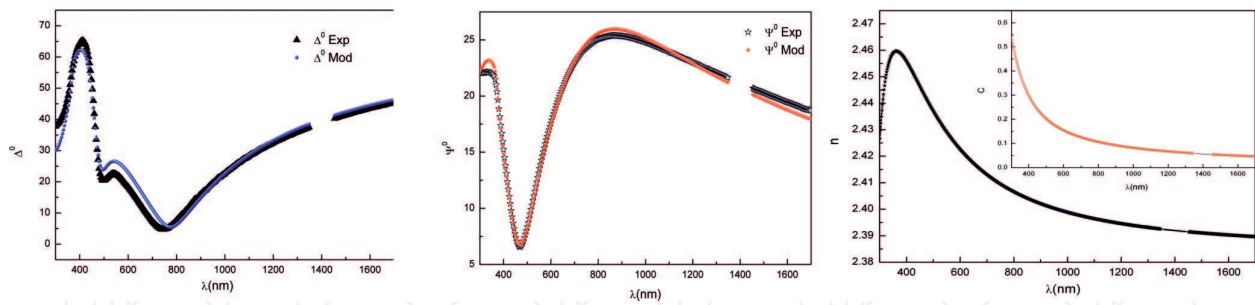
Figure 6. Experimental and model spectra for Δ (left) and Ψ (center) and refractive indices (n), and extinction coefficients (inset graph), for a thin film sample deposited at 266 nm laser wavelength [24].

3.1.6. Yttrium barium copper oxide (YBa$_2$Cu$_3$O$_{7-\delta}$)

YBa$_2$Cu$_3$O$_{7-\delta}$ (YBCO) is the famous high-temperature superconductive material, and it was extensively studied due to its superconducting properties. For appropriate oxygen content in the films, the maximum critical temperature T$_c$ can reach a value of 92 K. The application of YBCO thin films varies from electronic industry (microwave filters), military to medical devices (magnetic resonance imaging, Josephson junctions), or in sensor industry as highly sensitive magnetic field sensors (*SQUIDs*) [27, 28] and IR radiation sensors (bolometer). The superconducting properties of YBa$_2$Cu$_3$O$_{7-\delta}$ thin films are highly sensitive to the oxygen content. When δ varies between 0 ≤ δ ≤ 1, two symmetry phases can be observed, the tetragonal phase and the orthorhombic phase. For δ = 1, YBCO became an insulator, and for δ ≈ 0.1, this compound is a superconductor [29]. The epitaxial YBa$_2$Cu$_3$O$_{7-\delta}$ thin films have been obtained by PLD at high deposition temperature, usually around 780°C. For achieving the highest quality, the YBa$_2$Cu$_3$O$_{7-\delta}$ thin films need a postdeposition thermal treatment in oxygen atmosphere [30].

The deposition of YBCO thin films by pulsed laser deposition technique has been done by ablating a commercial YBCO ceramic target with an ArF excimer laser (λ = 193 nm) working at 5 Hz repetition rate. The thin films of YBCO was deposited on SrTiO$_3$ (001) single-crystal substrates [31]. Two sets of YBCO thin films have been deposited: first set was obtained by conventional PLD method and the second one by a hybrid technique where the PLD process is assisted by a radiofrequency-generated oxygen plasma plume (RF-PLD). For the first set of films, the following deposition parameters were used: laser fluency of 1.5 J/cm^2, oxygen pressure of 0.2 mbar, and substrate temperature of 780°C and target-substrate distance of 5 cm. The annealing treatments were done in the deposition chamber in two steps: 15 min at 650°C in 1 bar O$_2$ and 1 hour at 450°C in 1 bar of oxygen. The second set of samples was done by RF-PLD with or without postannealing treatments. The substrates were kept during deposition at 730°C, and the radiofrequency oxygen plasma beam working at 13.56 MHz and 200 W was used. The role of gas-discharge plasma (in oxygen) was to compensate the difference in deposition temperature.

Spectroscopic-ellipsometry measurements were performed between 300 and 1700 nm spectral range, with a step of 2 nm at 45, 60, and 75° angles of incidence. The optical model consists of three layers: the SrTiO$_3$ substrate, the YBCO layer, and a rough top layer considered to be

composed by 50% air and 50% YBCO in the Bruggeman effective medium approximation [11, 12]. The bulk dielectric function for the STO substrate was taken from literature [32]. In case of YBCO material, the dielectric function was described in detail by Kumar et al. [33] and is written as a sum of Lorentz and Drude terms.

The experimental data of Ψ and Δ for YBCO thin films were fitted with a sum of Lorentz oscillators for UV-VIS wavelengths and a Drude oscillator for near IR. The thickness of samples was found in the range of 120–150 nm, whereas the thickness of the top layer was 20–40 nm with an MSE value higher than 20. The roughness was in the same range with AFM results [31]. Because the ellipsometry is very sensitive at surface roughness, the large value of MSE can be explained by high value of roughness. In **Figure 7**, the experimental data and the fit results using the Lorentz-Drude model for the thin film of YBCO obtained by PLD at 780°C substrate temperature are presented.

From **Figure 7**, it is easy to observe the difference in the optical behavior for YBCO thin film growth in different conditions. For sample growth at 780°C, the normal optical behavior was
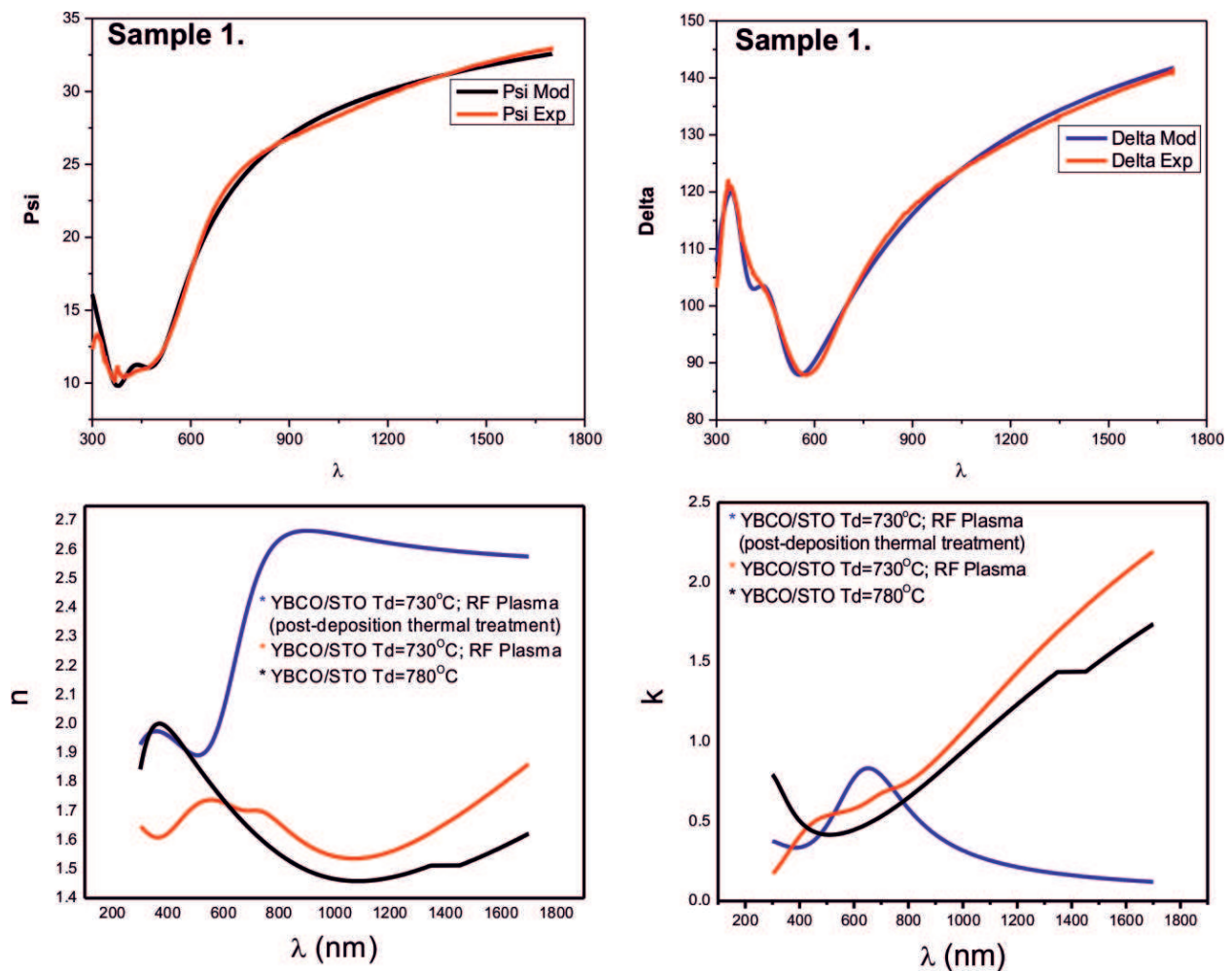
Figure 7. Comparison between the Lorentz and Drude fitting predictions and experimental measurements for YBCO thin film deposited by PLD and the refractive indices (left down) and extinction coefficient (right down) for YBCO thin films.

obtained [34]. In case of RF-PLD thin film growth at lower temperature (730°C) but in presence of oxygen RF discharge (without postannealing treatments), the value of refractive index and extinction coefficients are higher, and the optical behavior is different in the range of 250–600 nm. From XRD results, the YBCO films have an orthorhombic symmetry (a ~ 3.840 Å, b ~ 3.880 Å, and c ~ 11.688 Å) [31]. However, in case of RF-PLD deposition, the cell parameters were found to be a ~ 3.865 Å, b ~ 3.880 Å, and c ~ 11.70 Å, which means that the films were incompletely oxidized. The difference in the optical behavior can be explained by this difference in an oxidized state of YBCO layer.

For thin films deposited in the same way but with postannealing treatments in oxygen atmosphere, the dispersion of refractive index and extinction coefficients are completely different. This behavior is not characteristic for YBCO superconductor, and most probably, the amount of oxygen during deposition was too high.

As short conclusion of this study, the deposition parameters are very important especially when the properties of materials can be easily modified by the amount of certain chemical component, in our case the amount of oxygen in YBCO structure.

3.1.7. Strontium barium niobate

Strontium barium niobate (SBN) ($Sr_xBa_{1-x}Nb_2O_6$) is a ferroelectric material with tetragonal tungsten bronze structure without volatile chemical elements. SBN has pyroelectric activity as well as a large linear electro-optic (EO) coefficient(s) (r_{33} ~ 1300 p mV^{-1}) [34]. The high value of EO coefficient makes SBN an excellent candidate for electro-optic devices.

In the PLD experiment, the target of single-crystal SBN:60 (ce inseamna 60?) was ablated by a Surelite II Nd:YAG laser (λ = 265 nm). The repetition rate of the laser beam was set at 10 Hz. The laser fluency was varied in the 1.5–2.8 J/cm^2 range. The substrates, MgO$_{(001)}$ and Si$_{(100)}$, were placed at a distance of 4–5 cm from the target and were heated to the deposition temperature (600–700°C).

Spectroscopic ellipsometry measurements were performed in the visible and near-UV region of the spectrum, at energies between 1 and 5 eV, a step of 0.01 eV and at 65, 70, and 75° angles of incidence, with a step of 5°. The correlation between the energy and the wavelength scale of the spectrum is given by E = 1240/λ [12]. For the thin films of SBN deposited on Si substrates, the optical model consists of four layers: the silicon substrate, the native oxide (~3 nm), the SBN layer, and the rough top layer. In case of MgO substrate, the optical model was reduced to three layers: the MgO substrate, the SBN thin film, and the rough layer. In both cases, the dielectric function of the substrates is taken from literature and the rough top layer was approximated to consist of 50% air and 50% SBN in the Bruggeman approximation.

The film thickness and roughness were obtained by fitting the experimental data with a Cauchy dispersion model in the 1.2–2 eV range (620–1030 nm). In this range, the film is nonabsorbing (k ~ 0) and such dispersion is accepted. The thickness was found to be in the 150–250 nm range, and the MSE was found to be 3.8 for SBN/MgO and 2.5 for SBN/Si [35] (**Table 5**).

Samples	MSE	Thickness (nm)	An	Bn	Roughness (nm)
On MgO	3.741	165.935 ± 0.0418	2.0486 ± 0.000727	0.027885 ± 0.000728	2.215 ± 0.0428
On Si	2.559	227.304 ± 0.167	2.0418 ± 0.000943	0.024381 ± 0.000546	1.618 ± 0.121

Table 5. The fitting parameters obtained by Cauchy fit for SBN thin films [35].

In the next step, we replaced the Cauchy layer with a Tauc-Lorentz (T-L) oscillator. The T-L oscillator model was developed by Jellison and Modine and is used for amorphous materials [12], having the dielectric function (Eqs. (10) and (11)) written as:

$$\varepsilon = \varepsilon_1 + j\varepsilon_2 = (n + jk)^2 \tag{10}$$

with

$$\varepsilon_2 = \frac{AE_0C(E - E_g)^2}{(E^2 - E_0^2)^2 + C^2E^2}\frac{1}{E} \text{ for } E > E_g \text{ and } e_2 = 0 \text{ for } E \le E_g \tag{11}$$

where A, E_0, and C are dispersion parameters in the following limits: $E_0 > E_g$ and $C < 2E_0$.

For Tauc Lorentz oscillator, the real part of the dielectric function ε_1 is a (the) complete analytical solution to the Kramers-Kroning integral [12] (**Figure 8** and **Table 6**).

For the SBN thin film deposited on MgO and Si substrates, the values of refractive index and extinction coefficients were found to be smaller than for the crystalline target. The optical band gap, Eg, that results from Tauc-Lorentz fit is Eg = 3.81 eV for SBN on MgO substrate and Eg = 3.74 for SBN on Si substrate. The Eg value for single crystal target is Eg = 3.85 eV. From the XRD analysis, it results that all the samples made from the single-crystal targets are amorphous [35]. In this way, the smaller value of optical constants and value of band gap (Eg) can be explained because amorphous materials have lower refractive index than the same crystalline ones [12].

3.1.8. $Na_{1/2}Bi_{1/2}TiO_3-x\%BaTiO_3$

The solid solution of $(Na_{1/2}Bi_{1/2})TiO_3$ (BNT) with $BaTiO_3$ (BT) (BNT-BT) is considered to be a good alternative lead-free material to the PZT perovskite materials. (1-x) NBT-x BT shows a morphotropic phase boundary (MPB) between the rhombohedral and the tetragonal phase, at x between 0.06 and 0.07 [36]. The electrical and optical properties of NBT-xBT can be modified due to the phase transition from rhombohedral (R) to tetragonal (T).

A ceramic target of BNT-5%BT was ablated by a Surelite II Nd:YAG pulsed laser with wavelength of 266 nm, pulse duration of 5 ns and frequency 10 Hz, and a fluency of 1.6 J/cm². The number of laser pulses was 36,000. The films were grown on Pt/TiO₂/SiO₂/Si substrates, in reactive oxygen atmosphere at 0.1 mbar pressure. The distance between target and substrate was kept at 5 cm. During deposition, the substrates were heated at temperatures of 700 and 730°C.
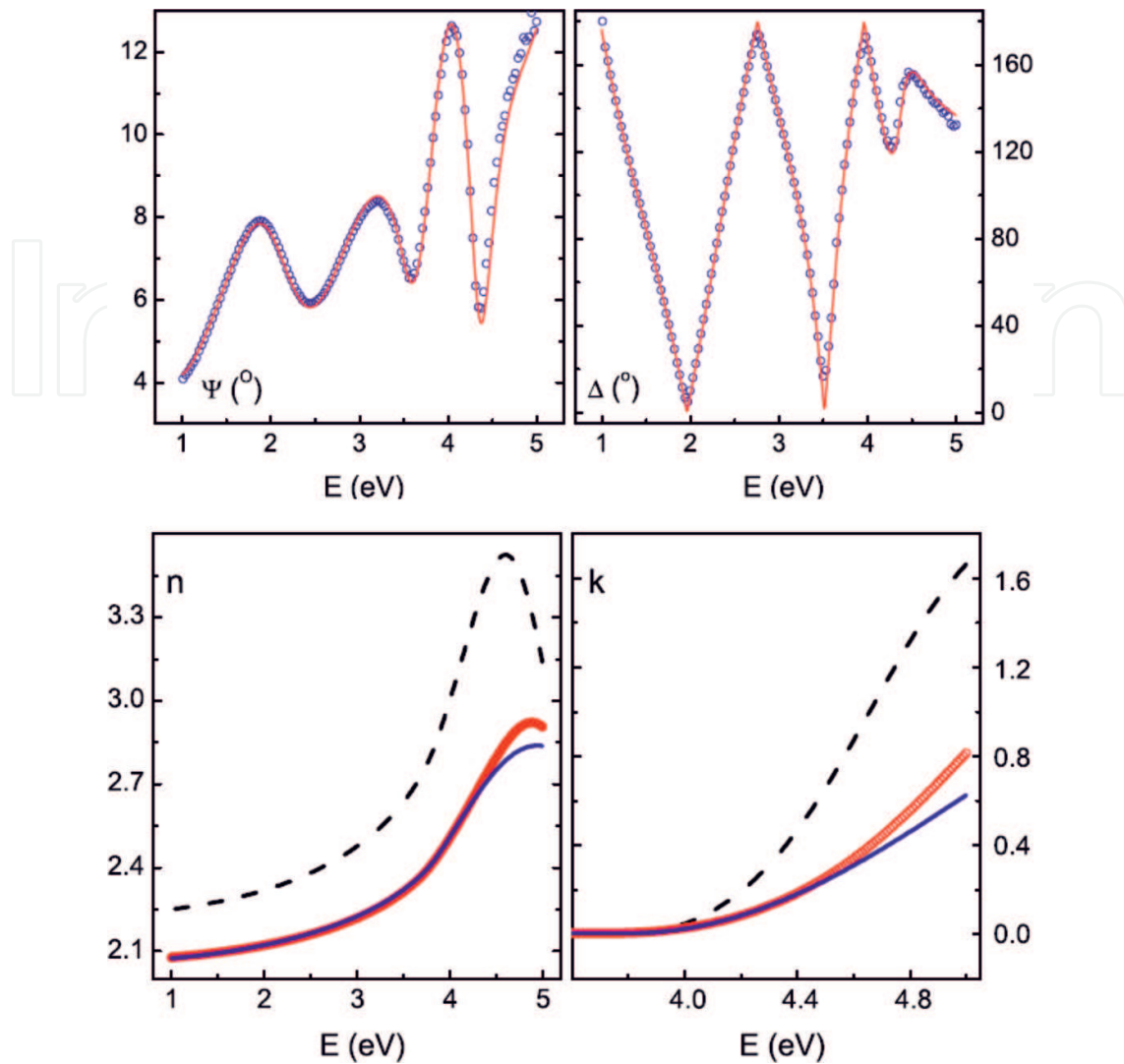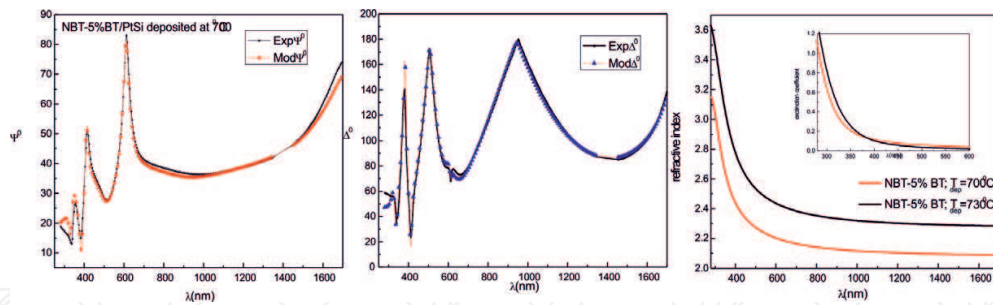
Figure 8. Ellipsometry spectrum for a-SBN on MgO. The circles represent the experimental data, whereas the solid lines result from the fitting procedure using the Tauc-Lorentz oscillator. (Down) Refractive index for crystalline target (dashed lines): a-SBN on MgO (red thick line) and a-SBN on Si (blue thin line) [35].

Samples	MSE	A	En	C	Eg	ε1
On MgO	8.094	193.1 ± 8.77	5.2978 ± 0.0393	3.2284 ± 0.162	3.8102 ± 0.0105	1.639 ± 0.0591
On Si	8.842	131.58 ± 8.34	5.2161 ± 0.0427	1.759 ± 0.163	3.7443 ± 0.0209	2.3611 ± 0.0893

Table 6. The fitting parameters obtained from Tauc-Lorentz fit [35].

For ellipsometric measurements, the angle of beam light incidence was set at 60–70° with a step of 5°. The experimental data of Ψ and Δ were acquired in the 250–1700 nm range of wavelength with a step of 2 nm. The optical model consists of three material layers: the platinum layer with a thickness of 150–200 nm, considered as a substrate; the BNT-5%BT thin film, and the roughness. As in the case of SBN, the fitting procedure consists of two steps: first, the thicknesses of thin films and the roughness were calculated from fitting the experimental data in the 600–1700 nm

Figure 9. Ellipsometry spectrum for BNT-5%BT on PT Si (left and center). The black lines represent the experimental data, whereas the dots result from the fitting procedure using the Gauss and Cody-Lorentz oscillator; the calculated refractive index and extinction coefficient (inset) for BNT-5%BT (right) deposited at substrate temperature of 700 (dots) and 730°C (lines) [40].

range of wavelength, and second, the Cauchy layer was replaced by an oscillator. In case of BNT-5%BT, the best fit was obtained using a sum of Gauss and Cody-Lorentz oscillator [37], a well-known optical model for BNT and solid solution BNT−x%BT [38, 39]. The thickness of samples was found to be d = 131.9 nm for BNT-5BT growth at 700°C, with a roughness of 26.9 nm, and for a film growth at 730°C, the thickness was 241.2 nm with a roughness of 23.7 nm. The values of MSE was 78.8 in case of Tdep = 700°C and 91.34 for Tdep = 730°C. In **Figure 9**, the Cody-Lorentz fit result and the calculated optical constants are presented.

The results of XRD indicate a polycrystalline randomly oriented thin films of BNT-BT growth by PLD on Pt/Si substrate [40]. The polycrystalline nature of BNT-BT thin film with randomly oriented nanocrystals can explain the high value of MSE. From **Figure 9**, it is easy to observe the discrepancy in modeled and experimental data in UV range, and this discrepancy can be caused by existence of small defects in sample. In terms of refractive index, the highest value was obtained for higher deposition temperature. The extinction coefficients "k" increase fast in the wavelength ranging from 280 to 380 nm. In the 380–600 nm spectrum range, the "k" presents an Urbach tail and this can be explained by optical scattering on randomly oriented nanocrystals.

4. Conclusions

Thin films of amorphous and crystalline oxides (Sm_2O_3, ZrO_2, $Sr_xBa_{1-x}Nb_2O_6$ (SBN), $Na_{1/2}Bi_{1/2}TiO_3$−x%$BaTiO_3$ (NBT-x%BT), high-temperature superconductive oxide $YBa_2Cu_3O_{7-\delta}$ (YBCO), and magnetic alloy (NdFeB) have been grown by pulsed laser deposition. The optical properties of films were successfully determined by spectroscopic ellipsometry. High transparent thin film was obtained in case of ZrO_2. The films of SBN and NBT-x%BT show a high value of refractive index (n > 2) and low extinction coefficients (k < 10^{-4}) in visible and near-IR range of wavelength. In our optical models presented above, we have to choose every time a different oscillator to describe the behavior of complex refractive index, and this choice was conducted by applying two rules: the "rule" of MSE—the smallest values of MSE mean the better fit, and in order to obtain the smallest value, a sum of oscillators can be tried until the experimental data and the theoretical data are overlapped. Second, we have to look at the types and properties of an initial material. The Lorentz oscillator have a symmetric shape, and the high

and low energy sides of the function decrease at the same rate and can be used for complex refractive index of conductive oxides or metal [41, 42]. The Lorentz oscillators have long asymptotic tail and cause unwanted absorption in transparent regions for some types of materials. The long tail of Lorentz oscillator was the reason for Lorentz fit in case of NdFeB alloy. In case of ferroelectric materials, the Lorentz does not fit very well because of the characteristics of the complex dielectric function at the near ultraviolet and ultraviolet (UV). For ferroelectric materials, the Tauc-Lorentz [43] or Cody-Lorentz oscillators are more flexible at higher energies in the ultraviolet range of the spectrum. The Tauc-Lorenz oscillator is used for amorphous ferroelectric materials, and this was the reason for choosing it in case of SBN thin film. For BNT-BT material, a Cody-Lorentz combined with a Gaussian oscillator will give the best results.

Acknowledgements

Author details

Valentin Ion*, Andreea Andrei, Maria Dinescu and Nicu Doinel Scarisoreanu

*Address all correspondence to: valentin.ion@inflpr.ro

National Institute for Laser, Plasma and Radiation Physics, Romania

References

[1] Maissel LI, Clang R. Handbook of Thin Film Technology. New York: McGraw-Hill; 1970

[2] Bunshah RF. Deposition technologies for Films and Coatings: Developments and Applications. Park Ridge, NJ: Noyes Publications; 1982

[3] Maiman TH. Optical and microwave-optical experiments in ruby. Physical Review Letters. 1960;**4**:564

[4] Smith HM, Turner AF. Vacuum deposited thin films using a ruby laser. Applied Optics. 1965;**4**:147-148. DOI: 10.1364/AO.4.000147

[5] Chrisey DB, Hubler GK. Pulsed Laser Deposition of Thin Films. Wiley-Interscience; 1 edition (June 7, 1994); ISBN-13: 978-0471592181

[6]   Ghandhi SK. VLSI Fabrication Principles: Silicon and Gallium Arsenide. New York: John Wiley & Sons; 1983

[7]   Losurdo M, Hingerl K. Ellipsometry at the Nanoscale. Berlin Heidelberg: Springer-Verlag; 2013. DOI: 10.1007/978-3-642-33956-1

[8]   Azzam RMA, Bashara NM. Ellipsometry and Polarized Light. New York, NY, USA: North-Holland Publishing Co; 1977

[9]   Adams JR, Bashara NM. Determination of the complex refractive index profiles in P+31 ion implanted silicon by ellipsometry. Surface Science. 1975;**49**(2):441-458

[10]   Tompkins HG. A User's Guide to Ellipsometry. San Diego, CA, U.S.A: Academic Press Inc.; 1993. ISBN 978-0-126-93950-7

[11]   Tompkins HG, Irene EA. Handbook of Ellipsometry. Norwich, NY, U.S.A.: William Andrew Publishing/Noyes; 2005. ISBN 978-0-815-51499-2

[12]   Fujiwara H. Spectroscopic Ellipsometry: Principles and Applications. John Wiley & Sons, Ltd: Chichester, UK; 2007 978-0-470-01608-4

[13]   Azzam RMA. Ellipsometry. In: Bass M, editor. Handbook of Optics. Geometrical and Physical Optics, Polarized Light, Components and Instruments. Vol. 1. 3rd ed. New York, NY, USA.: McGrow-Hill Companies, Inc; 2010. p. 16.1–16.25. ISBN 978-0-071-62925-6

[14]   Aspnes DE, Theeten JB, Hottier F. Investigation of effective-medium models of microscopic surface roughness by spectroscopic ellipsometry. Physical Review B. 1979;**20**:3292-3302

[15]   Dakhel AA. Dielectric and optical properties of samarium oxide thin films. Journal of Alloys and Compounds. 2004;**365**(1–2):233-239. DOI: 10.1016/S0925-8388(03)00615-7

[16]   Yang H, Wang H, Luo HM, Feldmann DM, Dowden PC, DePaula RF, Jia QX. Structural and dielectric properties of epitaxial Sm_2O_3 thin films. Applied Physics Letters. 2008;**92**: 062905. DOI: 10.1063/1.2842416

[17]   Herzinger CM, Johs B, McGahan WA, Woollam JA, Paulson W. Ellipsometric determination of optical constants for silicon and thermally grown silicon dioxide via a multi-sample, multi-wavelength, multi-angle investigation. Journal of Applied Physics. 1998; **83**:3323. DOI: 10.1063/1.367101

[18]   Constantinescu C, Ion V, Galca AC, Dinescu M. Morphological, optical and electrical properties of samarium oxide thin films. Thin Solid Films. 2012;**520**(20):6393-6397. DOI: 10.1016/j.tsf.2012.06.049

[19]   Wilk GD, Wallance RM, Anthony JM. High-κ gate dielectrics: Current status and materials properties considerations. Journal of Applied Physics. 2001;**89**:5243-5275. DOI: 10.1063/1.1361065

[20]   Zhamg W, Gan J, Hu Z, Yu W, Li Q, Sun J, Xu N. Infrared and Raman spectroscopic studies of optically transparent zirconia (ZrO_2) films deposited by plasma-assisted reactive pulsed laser deposition. Applied Spectroscopy. 2011;**65**(5):522-527

[21] Cancea VN, Birjega R, Ion V, Filipescu M, Dinescu M. Analysis of zirconia thin films grown by Pulsed Laser Deposition. Physics AUC. 2012;**22**:50-62

[22] Yamashita S, Yamasaki J, Ikeda M, Iwabuchi N. Anisotropic Nd–Fe–B thin-film magnets for milli-size motor. Journal of Applied Physics. 1991;**70**:6627. DOI: 10.1063/1.349879

[23] Nakano M, Sahara M, Yanai T, Yamashita F, Fukunaga H. Nd–Fe–B thick film magnets with Nb additive prepared by vacuum arc deposition method. Journal of Applied Physics. 2011;**109**:07A755. DOI: 10.1063/1.3566061

[24] Constantinescu C, Scarisoreanu N, Moldovan A, Dinescu M, Petrescu L, Epureanu G. Thin films of NdFeB deposited by PLD technique. Applied Surface Science. 2007;**253** (19):8192-8196. DOI: 10.1016/j.apsusc.2007.02.165

[25] Liu W, Zhang Z, Liu J, Chen HL, Liu LY, Sun X, Sellmyer D. Exchange coupling and remanence enhancement in nanocomposite multilayer magnets. Advanced Materials. 2002;**14**(24):1832-1834. DOI: 10.1002/adma.200290012

[26] Constantinescu C, Ion V, Codescu M, Rotaru P, Dinescu M. Current Applied Physics. 2013;**13**:2019-2025. DOI: 10.1016/j.cap.2013.09.002

[27] Koelle D, Kleiner R, Ludwig F, Dantsker E, Clarke J. Reviews of Modern Physics. 1999;**71**:631

[28] Sekitani T, Miura N, Ikeda S, Matsuda YH, Shiohara Y. Upper critical field for optimally-doped $YBa_2Cu_3O_{7-\delta}$. Physica B: Condensed Matter. 2004;**346–347**:319. Bibcode:2004Phy B01.098. DOI: 10.1016/j.physb.2004

[29] Pedarnig JD, Göttlich H, Rössler R, Heckl WM, Bäuerle D. Patterning of $YBa_2Cu_3O_{7-\delta}$ films using a near-field optical configuration. Applied Physics A: Materials Science & Processing. 1998;**67**:403-405

[30] Kusumori T, Muto H. Influence of target composition on the quality of YBCO films fabricated by Nd:YAG pulsed laser deposition. Physica C. 2001;**351**:227-244

[31] Stanciu G, Scarisoreanu ND, Ion V, Moldovan A, Andronescu E, Dinescu M. Ba2Cu3O7-δ thin films deposited by pulsed laser deposition and radio-frequency assisted pulsed laser deposition. Journal of Optoelectronics and Advanced Materials. September–October 2012;**14**(9–10):852-857

[32] Palik ED. Handbook of Optical Constants of Solids. Vol. II. p. 1035-1048, Academic Press; 1 edition (April 4, 1991), ISBN-13: 978-0125444224

[33] Kumar AR, Zhang ZM, Boychev VA, Tanner DB, Vale LR, Rudman DA. Far-infrared transmittance and reflectance of $YBa_2Cu_3O_{7-s}$ films on Si substrates. Journal of Heat Transfer. 1999;**121**:844-851

[34] Hesselink L, Bashaw MC. Optical memories implemented with photorefractive media. Optical and Quantum Electronics. 1993;**25**(9):S611-S661. DOI: 10.1007/BF00444334

[35] Ion V, Galca AC, Scarisoreanu ND, Filipescu M, Dinescu M. Spectroscopic ellipsometry study of amorphous SrxBa1−xNb2O6 thin films obtained by pulsed laser deposition. Physica Status Solidi (c). 2008;**5**(5):1180-1183. DOI: 10.1002/pssc.200777818

[36] Takenaka T, Maruyama K, Sakata K. (Bi1/2Na1/2)TiO3-BaTiO3 system for lead-free piezoelectric ceramics. Japanese Journal of Applied Physics. 1991;**30**:2236

[37] Ferlauto AS, Ferreira GM, Pearce JM, Wronski CR, Collins RW, Deng X, Ganguly G. Analytical model for the optical functions of amorphous semiconductors from the near-infrared to ultraviolet: Applications in thin film photovoltaics. Journal of Applied Physics. 2002;**92**:2424. DOI: 10.1063/1.1497462

[38] Cernea M, Trupina L, Dragoi C, Galca A-C, Trinca L. Structural, optical, and electric properties of BNT–BT0.08 thin films processed by sol–gel technique. Journal of Materials Science. 2012;**47**(19):6966-6971. DOI: 10.1007/s10853-012-6646-1

[39] Dorywalski K, Lemée N, Andriyevsky B, Schmidt-Grund R, Grundmann M, Piasecki M, Bousquet M, Krzyzynski T. Optical properties of epitaxial Na0.5Bi0.5TiO3lead-free piezoelectric thin films: Ellipsometric and theoretical studies. Applied Surface Science. 2016:18. DOI: 10.1016/j.apsusc.2016.09.078

[40] Scarisoreanu N, Craciun F, Ion V, Birjega R, Dinescu M. Structural and electrical characterization of lead-free ferroelectric Na1/2Bi1/2TiO3–BaTiO3 thin films obtained by PLD and RF-PLD. Applied Surface Science. 2007;**254**(4):1292-1297. DOI: 10.1016/j.apsusc.2007.09.036

[41] Synowicki A. Spectroscopic ellipsometry characterization of indium tin oxide film microstructure and optical constants. Thin Solid Film. 1998;**313–314**:394-397. DOI: 10.1016/S0040-6090(97)00853-5

[42] Brevnov DA, Bungay C. Diameter-dependent optical constants of gold mesoparticles electrodeposited on aluminum films containing copper. The Journal of Physical Chemistry B. 2005;**109**(30):14529-14535. DOI: 10.1021/jp0511707

[43] Jellison GE, Modine FA. Parameterization of the optical functions of amorphous materials in the interband region. Applied Physics Letters. 1996;**69**:2371. DOI: 10.1063/1.118064